Available online at www.sciencedirect.com

ScienceDirect

Journal of the European Ceramic Society 35 (2015) 803–812

www.elsevier.com/locate/jeurceramsoc

Characterization of aluminum hydroxide ($Al(OH)_3$) for use as a porogenic agent in castable ceramics

Adriane D.V. Souza [a], Cezar C. Arruda [a], Leandro Fernandes [a], Maria L.P. Antunes [b], Pedro K. Kiyohara [c], Rafael Salomão [a,*]

[a] *Materials Engineering Department, São Carlos School of Engineering, University of São Paulo, Avenida Trabalhador São-carlense 400, 13566-590 São Carlos, SP, Brazil*

[b] *Environmental Engineering Department, UNESP – Universidade Estadual Paulista, Avenida Três de Março 511, Sorocaba, SP, Brazil*

[c] *General Physics Department, Physics Institute, University of São Paulo, Rua do Matão, Travessa R, 187 Cidade Universitária, CP 66318 São Paulo, SP, Brazil*

Received 19 July 2014; received in revised form 4 September 2014; accepted 7 September 2014
Available online 26 September 2014

Abstract

Porous structures based on aluminum oxide-hydroxide (Al_2O_3-$Al(OH)_3$) show high refractoriness. Regarding their use as thermal insulators, the preparation of aqueous castable suspensions requires suitable conditions to produce stable co-dispersions and a deeper knowledge on their porogenic-sintering behaviors. This study reports on the characterization of a commercial grade of $Al(OH)_3$ and several transition phases of Al_2O_3 (attained through the calcination of $Al(OH)_3$) aiming at their use as porogenic agents for castable porous ceramics. X-ray diffraction, thermogravimetry, Helium picnometer method, specific surface area and electron microscopy were used. The dispersion and rheology of $Al(OH)_3$ and Al_2O_3 were investigated with pH variations and dispersants. Aluminum oxide and hydroxide particles showed high compatibility in aqueous medium and favored the preparation of suspensions. As porogenic agents, the transition phases showed a large quantity of meso-macro pores and a huge variation in the specific surface area, which highlight their potential to produce high refractoriness porous structures.

Keywords: Aluminum hydroxide; Aluminum oxide; Transition phases; Dispersion; Rheology

1. Introduction

Aluminum hydroxide ($Al(OH)_3$) has been used as anti-flame additive for polymers, abrasive medium for soft polishing operations (in toothpaste, for instance), as a precursor for catalysts and in filters for water treatment.[1–4] Nevertheless, it has been mostly applied in the production of metallic aluminum through the electrolysis of aluminum oxide (Al_2O_3), attained after its calcination.[2] The most common route to produce $Al(OH)_3$ is known as Bayer process and bauxite (composed mainly of $Al(OH)_3$) and impurities such as SiO_2, Fe_2O_3 and TiO_2 is its main raw material.[1,4] Initially, bauxite is dissolved in a hot (70–90 °C) NaOH solution for the formation of sodium aluminate, according to the general expression:

$$\text{Bauxite}(Al(OH)_3 + \text{impurities}) + NaOH \rightarrow Na_2Al_2O_{4(\text{Dissolved})} + \text{impurities}_{(\text{Undissolved})} \quad (1)$$

After filtration steps for the removal of undissolved impurities, the clarified sodium aluminate solution is cooled down to precipitate $Al(OH)_3$:

$$Na_2Al_2O_{4(\text{Dissolved})} \rightarrow 2Al(OH)_{3(\text{Precipitated})} + NaOH_{(\text{Dissolved})} \quad (2)$$

After another filtering and washing steps, the NaOH solution can be recycled and the $Al(OH)_3$ pulp is spray-dried. Further heating in rotary kilns (1200–1600 °C) produces calcined alumina (α-Al_2O_3).

* Corresponding author. Tel.: +55 16 33739576; fax: +55 16 33739590.
E-mail addresses: rsalomao@sc.usp.br, rflslm@gmail.com (R. Salomão).

http://dx.doi.org/10.1016/j.jeurceramsoc.2014.09.010
0955-2219/

Table 1
Characteristics of the as-received raw materials.

Characteristics	Calcined alumina (α-Al_2O_3)[a]	Aluminum hydroxide ($Al(OH)_3$)[b]
Composition (wt%)	Al_2O_3: 99.8; Na_2O: 0.08; Fe_2O_3: 0.02; SiO_2: 0.03; CaO: 0.02; MgO: 0.07	$Al(OH)_3$: 99.7; Na_2O: 0.2; Fe_2O_3: 0.07; SiO_2: 0.03
Solid density ($g\,cm^{-3}$)	3.99 ± 0.07	2.42 ± 0.03
Specific surface area ($m^2\,g^{-1}$)	7.2 ± 1.0	5.8 ± 1.0
Particle size (D_{50}/D_{90}, μm)	0.61/1.03	0.89/1.19
Loss of ignition (wt%, 900 °C)	0.81	36.43

[a] CT3000SG.
[b] Hydral 710: Almatis, USA.

Due to its technological importance, the Al_2O_3-$Al(OH)_3$ system has been intensely investigated over the past decades and two fields, in particular, can be highlighted.

(1) The strong relationship between the $Al(OH)_3$ calcination conditions and the physic-chemical properties and microstructure of the Al_2O_3 phases produced.[5–10] The thermal decomposition of $Al(OH)_3$ is a complex process with an intense crystallographic rearrangement that occurs according to the general expression:

$$2Al(OH)_3 \rightarrow Al_2O_3 + 3H_2O \quad (3)$$

A 34 wt% mass loss can be observed in this stage due to the endothermic release of water vapor, followed by density increase and huge variation in the specific surface area (results above $300\,m^2\,g^{-1}$ are frequently reported)[7,11–13]. Several studies on the use of this system as a catalyst support have reported the effects of varying particle size distribution, impurities content, specific surface area, degree of crystallinity, heating rate (assisted or not by vacuum) and maximum temperature achieved.[10–12] By varying these parameters, significant differences can be observed in the atomic mobility and diffusivity of the precursor particles, which leads to different mass loss intensities and rates, specific surface area levels and phase changes temperature

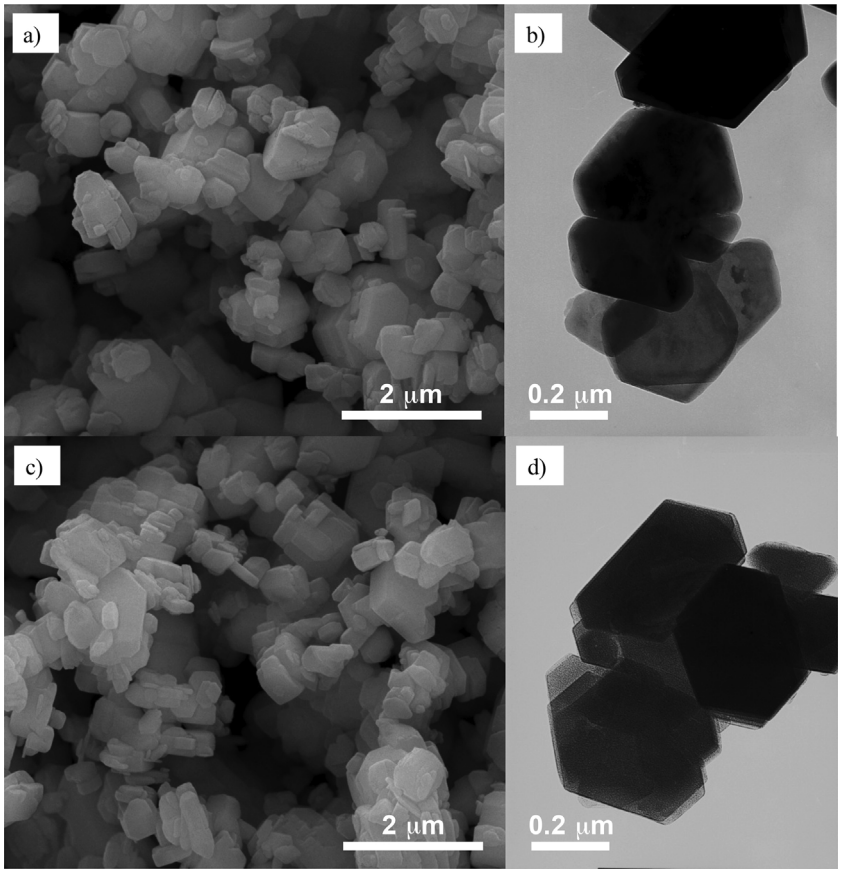

Fig. 1. SEM and TEM for $Al(OH)_3$ samples (a and b) as-received and (c and d) treated at 300 °C for 5 h.

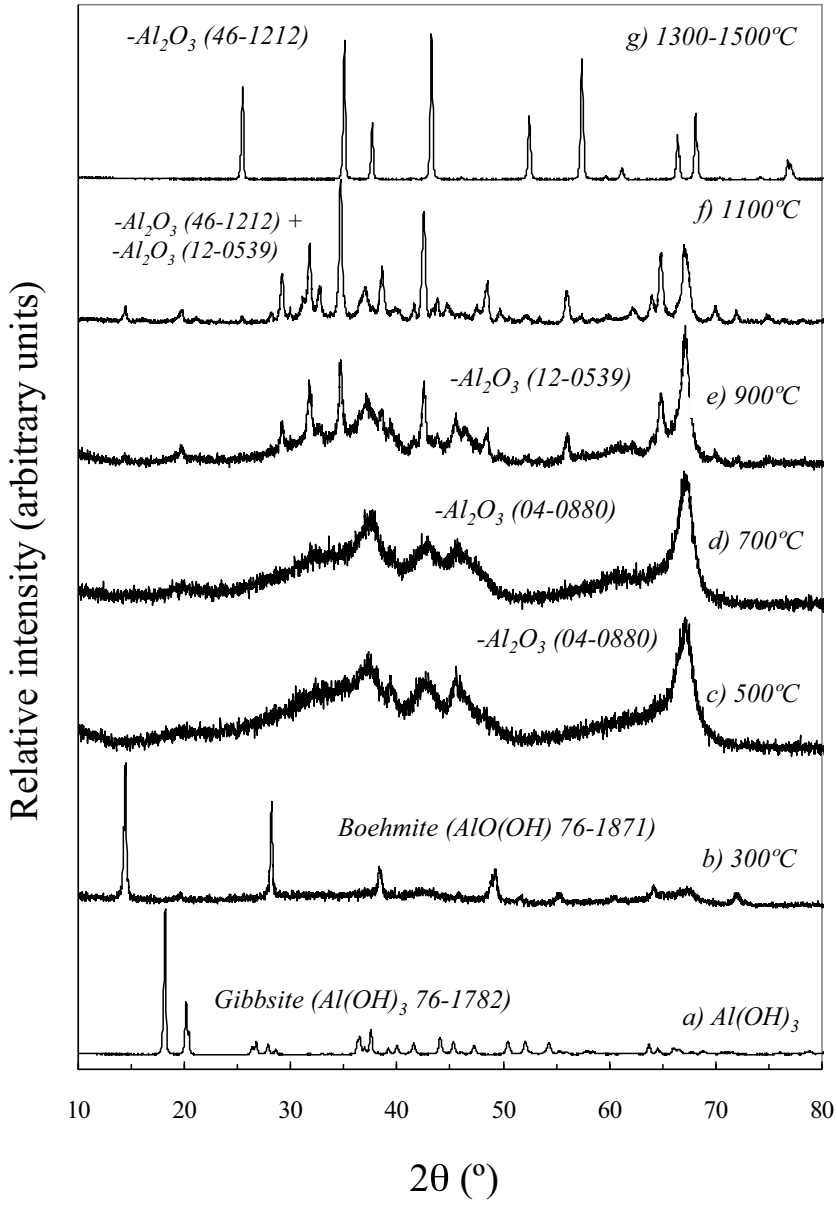

Fig. 2. X-ray diffraction patterns for samples of $Al(OH)_3$ calcined at different temperatures (5 °C min^{-1} heating rate, 5 h hold, 10 °C min^{-1} cooling rate). The numbers in brackets correspond to the JCPDS file used for identification.

interval. The term transition alumina describes a family of compounds formed at the end of the dehydroxilation of $Al(OH)_3$ and before the total stabilization as α-Al_2O_3 and has been intensely explored.[7,12] Such phases are based on a fixed face-centered cubic array of oxygen anions where aluminum cations, placed at their interstices, can be rearranged at different extents, depending on the temperatures involved. For instance, transition aluminas attained from the flash calcination (heating rates higher than 100 °C s^{-1}) of gibbsite can produce low crystallinity and defect-rich phases (such as ρ-Al_2O_3),[14–16] whereas, when the material is gradually decomposed in the same temperature interval, crystalline phases (χ-Al_2O_3 and κ-Al_2O_3) are attained.[6,7,10]

(2) Porous structures based on the Al_2O_3-$Al(OH)_3$ system have found applications in hot gas filtration,[3] scaffolds for growing biological tissues and microorganisms,[17] biomaterial for bone replacement[18] and thermal insulation.[19–22] To produce such structures, $Al(OH)_3$ particles (in contents of up to 90 wt%) must be inserted into a dense calcined or tabular alumina matrix (comprised by α-Al_2O_3) and consolidated by pressing[19] or using binding agents.[18,21,22] After the $Al(OH)_3$ decomposition, high-porosity structures are attained due to the loss of water and the large volume of micro- and meso-pores formed on their surface.[19] Moreover, these phase transformations are strongly affected by the seeding effect of the surrounding α-Al_2O_3 particles. In the presence of calcined or tabular alumina, the transition phases are converted to α-Al_2O_3 at temperatures below 1000 °C, which leads to an early sintering.[6,21,22] The porosity levels remain high up to 900 °C, when the pores and

cracks begin to disappear as the transition alumina structure heals. The presence of highly reactive transition alumina particles also induces the grain growth of the α-Al_2O_3 ones during the sintering.[18] The latter effect is the main limitation of porous Al_2O_3-$Al(OH)_3$ structures regarding their use as a thermal barrier for applications in which temperature ranges are above 1000 °C for long periods, despite their high refractoriness.

For both fields, some aspects related to the processing conditions that could enhance the technological use of the system have received less attention in the recent literature, specially considering commercial or non-analytical grades. Therefore, the present study provides novel insights on: (1) the dispersion, rheological and Zeta potential behavior of $Al(OH)_3$ and Al_2O_3 suspensions (to produce more homogeneous mixings and finer

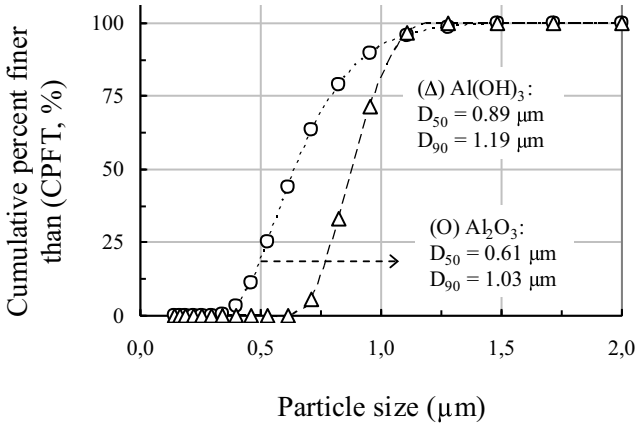

Fig. 3. Particle size distribution of the $Al(OH)_3$ and Al_2O_3 samples tested.

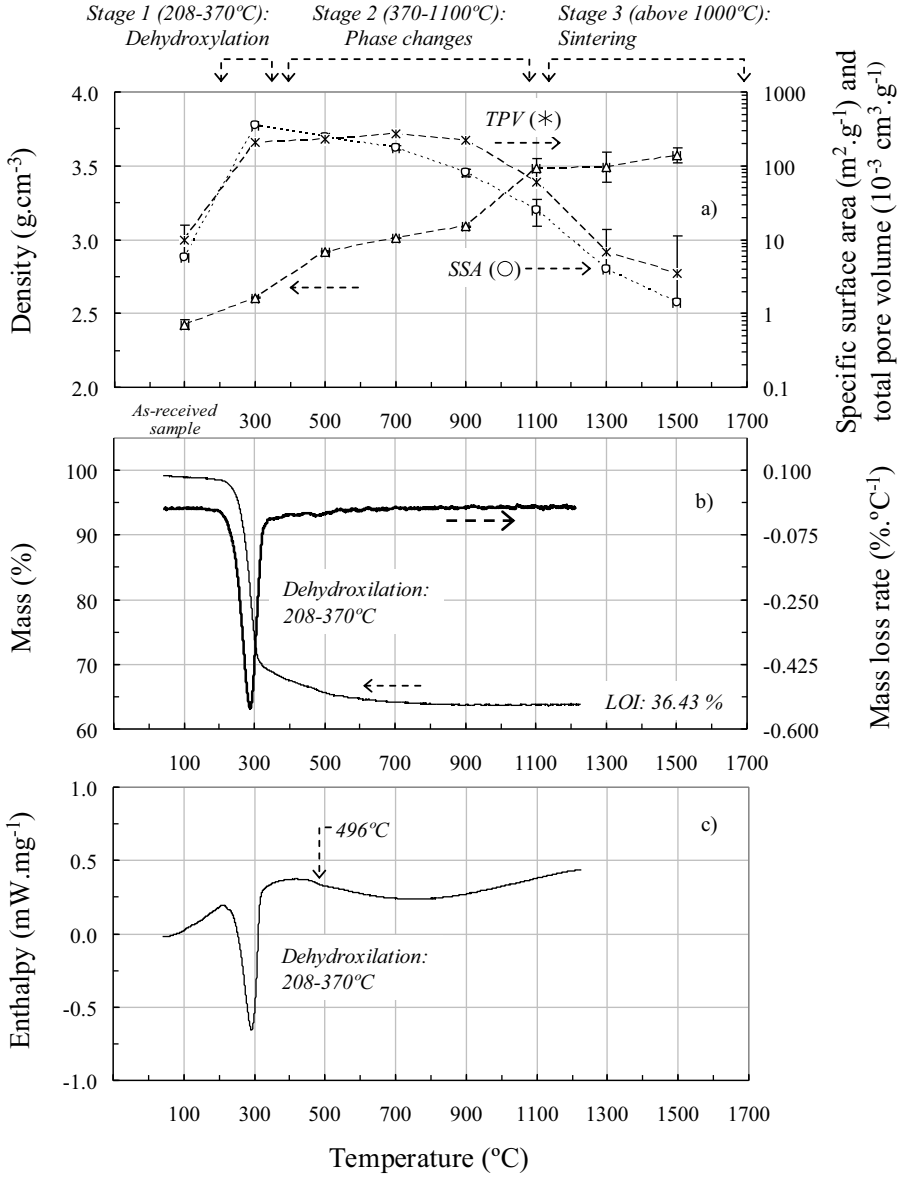

Fig. 4. (a) Density (Helium picnometry), specific surface area (SSA, BET method) and total pore volume (TPV, N_2 adsorption method) for samples of $Al(OH)_3$ calcined at different temperatures (5 °C min^{-1} heating rate, 5 h hold, 10 °C min^{-1} cooling rate); (b) thermogravimetric analysis (TGA) and (c) differential scanning calorimetry (DSC) for $Al(OH)_3$ (5 °C min^{-1} heating rate).

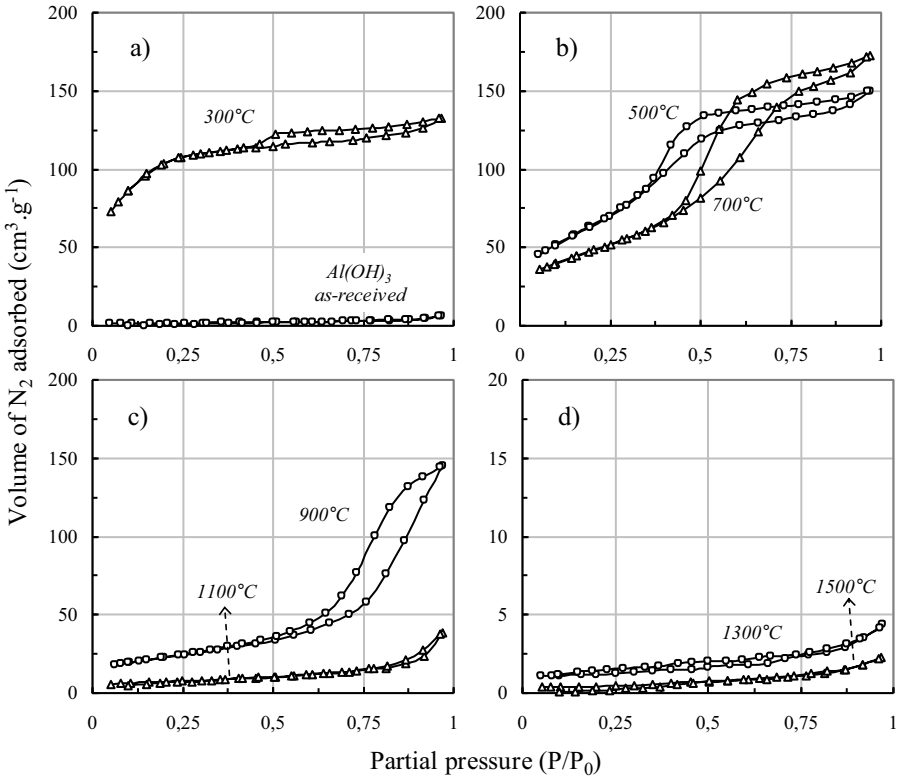

Fig. 5. Adsorption/desorption isotherms for $Al(OH)_3$ samples calcined at different temperatures (5 °C min^{-1} heating rate, 5 h hold, 10 °C min^{-1} cooling rate).

microstructures); (2) the thermal decomposition of $Al(OH)_3$ (to enable safer and faster heating schedules to produce transition aluminas); (3) the sintering behavior of transition alumina particles and the densification of their micro- and meso-porosity (to produce structures of higher porosity and improved thermomechanical properties).

2. Experimental

The aluminum hydroxide employed in the tests (Hydral 710, Almatis, Germany) is a high-purity commercial grade originally used as an anti-flame agent and reinforcement in polymeric composites. Calcined alumina (CT3000 SG, Almatis, Germany) of similar particle size distribution was tested as a reference under the same conditions. The as-received raw materials (Table 1) were physically characterized as follows: (a) Composition (X-ray dispersive spectroscopy, Shimadzu, EDX 720, Japan); (b) Solid density (ρ_{Solid}) was determined by Helium pycnometer method (Ultrapyc 1200e, Quantachrome Instruments, USA; samples were previously dried overnight at 110 °C); (c) specific surface area (SSA, Nova 1200e, Quantachrome Instruments, USA, ASTM C1069-09) was measured by BET method (samples were previously degassed at 200 °C for 3 h, prior to each measurements; 99.999% purity N_2 was employed as the adsorption gas; P/P_0 varied from 0.05 up to 0.3); (d) the loss of ignition (LOI) was attained for samples dried overnight at 110 °C and after calcination at 900 °C, for 5 h, at 5 °C min^{-1} heating rate.

Aqueous suspensions containing 30 vol.% of solid of each raw material were individually prepared in a paddler mixer (PowerVisc, Ika, Germany) with no dispersant and at 1000 rpm for 5 min. After the addition of small amounts of dispersants (ammonium citrate dibasic, $HOC(CO_2H)(CH_2CO_2NH_4)_2$, DAC, Sigma; and poly(ethylene glycol)-based, FS20 Castment, BASF, Germany), the suspensions were homogenized for 60 s. Their apparent viscosities (η, Pa s) were measured (Brookfield Viscosimeter, VLDV-II + PRO, USA) with a coaxial cylinder configuration (barrel: 19 mm diameter by 65 mm length and spindle 17.47 mm diameter by 31.85 mm height) at a 50 s^{-1} shear rate for 60 s (this period had been previously determined as sufficient for the achievement of steady-state conditions). The apparent viscosity of the suspensions were measured in shear rate cycles from 0.15–80–0.15 s^{-1} (the same solid content, 30 vol.%, was employed in these tests) and using the optimum dispersant (FS20) content previously determined for each raw material

The Zeta potential of the $Al(OH)_3$ and Al_2O_3 particles was measured in different pH ranges and using 2 vol.% of diluted aqueous suspensions (DT-1202, Dispersion Technology Inc., USA) containing DAC or FS20 (optimum content previously determined by viscosimetry). A 2-min sonication was applied to improve particle individualization. The pH was continuously shifted toward acid and alkaline ranges using 0.5 M NH_4OH and HCl solutions, with a 1-min interval between each measurement for stabilization. The particle size distribution (D_{50}/D_{90}, μm) was determined for the suspension containing the optimum dispersant content (DAC) at pH 10 (DT-1202, Dispersion Technology Inc., USA). During the dispersion and rheological tests and Zeta potential measurements, the temperature of the

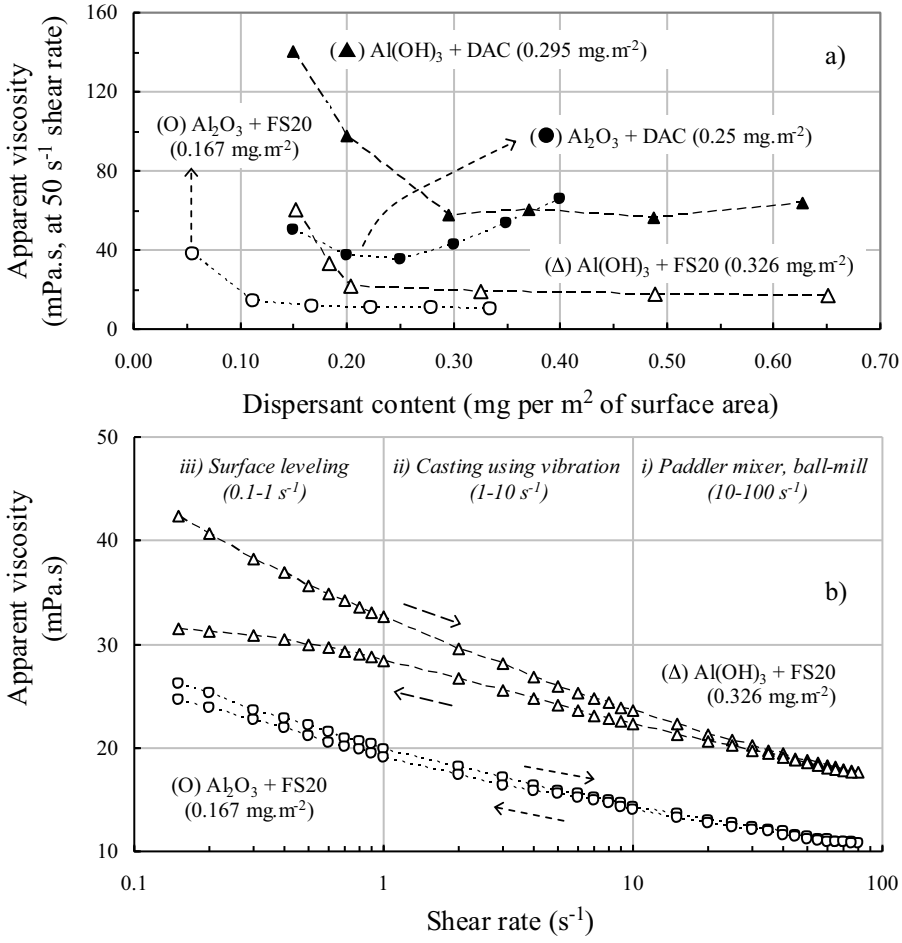

Fig. 6. (a) Effect of dispersants (ammonium citrate dibasic, DAC, and poly(ethylene glycol)-based, FS20) on $Al(OH)_3$ and Al_2O_3 aqueous suspensions (the numbers in brackets indicate the ideal dispersant content for a minimum apparent viscosity); (b) effect of shear rate on the apparent viscosity for $Al(OH)_3$ and Al_2O_3 aqueous suspensions (containing the ideal FS20 content).

suspensions was kept at 25 °C ± 0.5 °C (thermal bath, Brookfield TC-550, USA).

The modifications produced in the $Al(OH)_3$ powder by heating and sintering were evaluated by thermogravimetry (TGA-Q50, TA Instruments, 25–1250 °C, and synthetic air atmosphere) and differential scanning calorimetry (DSC 404, Netzsch, Germany) of the as-received powder up to 800 °C, at a 5 °C min^{-1} heating rate. The powder was then treated at 300–1500 (5 °C min^{-1} heating rate, 5 h hold, 15 °C min^{-1} cooling rate). For each condition, the solid density, specific surface area and total volume of pores were measured (samples had been previously degassed at 200 °C for 3 h prior to each measurement; 99.999% purity N_2 was employed as the adsorption gas and P/P_0 ranged from 0.05 up to 1; for the as-receive samples, the degassing step was carried out at 100 °C for 24 h).

The phases formed attained at each temperature were identified by X-ray diffraction (Rotaflex RV 200B, Rigaku-Denki Corp., Japan; with Kα ≡ Cu radiation, λ ≡ 0·15406 nm, in the 2θ range from 3° to 100° at a 2° min^{-1} scan rate). The X-ray data were compared with JCPDS files. Their microstructures were observed by field emission gun scanning electron microscopy (SEM, FEI 7500F, 30 kV, samples were placed upon stubs and covered with gold) and transmission electron microscopy (TEM, Philips CM200, 200 kV, samples were dispersed on carbon covered grids).

3. Results and discussion

3.1. Synthesis, morphology and dispersion and rheological behavior of the as-received $Al(OH)_3$

The $Al(OH)_3$ particles used in this study (Fig. 1a and b) are a highly crystalline form of gibbsite (Fig. 2a) of regular hexagonal plate-like shape and narrow size distribution (Fig. 3). They are also dense (Fig. 4a and Table 1) with practically no inner porosity (Fig. 5a). These characteristics have been reported in many studies on the synthesis of particles and nanoparticles by wet precipitation methods.[12,23,24]

$Al(OH)_3$ and Al_2O_3 (tested as reference) suspensions were suitably dispersed with ammonium citrate dibasic (DAC) and poly(ethylene glycol)-based additive (FS20) and required, respectively, 0.295 mg and 0.326 mg of additive per m^2 of surface area (Fig. 6a). To the best of our knowledge, no similar result has been found in the literature for $Al(OH)_3$ dispersion; on the other hand, the Al_2O_3 tested as reference has shown an optimum dispersant content similar to those found

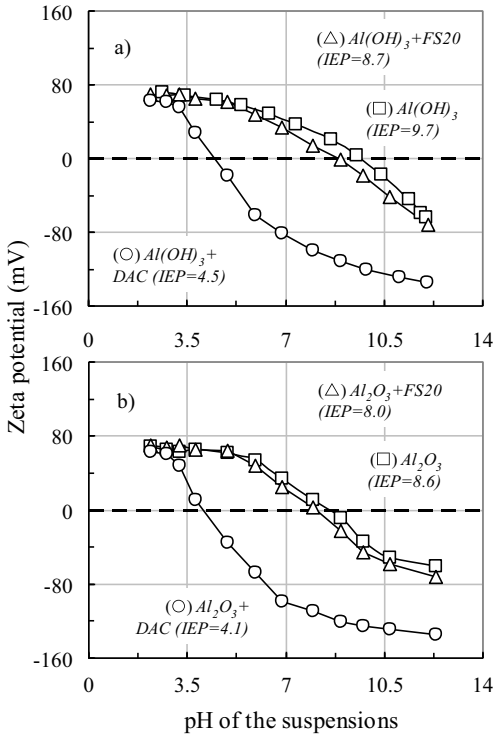

Fig. 7. Zeta potencial *vesus* pH behavior of (a) $Al(OH)_3$ and (b) Al_2O_3 suspensions dispersed with DAC and poly(ethylene glycol)-based additive (FS20). The optimum dispersant contents showed in Fig. 6 were employed for each test.

in other reports (0.25 mg and 0.167 mg per m^2 of surface area, respectively).[25–27] The similarities of the Zeta potential behavior between $Al(OH)_3$ (Fig. 7a) and Al_2O_3 (Fig. 7b) particles can be explained considering two aspects: 1 in contact with water, fine calcined Al_2O_3 particles rapidly develop a hydroxilated coating on their surfaces chemically similar to $Al(OH)_3$.[12,18] 2 Such particles also show similar average particle size and specific surface area (0.66 μm and 0.89 μm and 7.2 $m^2\ g^{-1}$ and 5.8 $m^2\ g^{-1}$, respectively), responsible for a similar charge density and distribution on their surfaces.

Regarding the differences about each dispersant effects, it can be pointed out that the apparent viscosity levels achieved were significantly lower for the suspensions containing FS20. Moreover, whereas FS20 did not affect the Zeta potential versus pH behavior of the suspensions significantly, DAC shifted the isolectric point of $Al(OH)_3$ and Al_2O_3 to lower pH ranges (from 9.7 to 4.5 and 8.6 to 4.1, respectively, Fig. 7). In pH ranges from neutral to alkaline, citrate-based dispersants, such as citric acid, sodium citrate and DAC, dissociate their hydroxyl (OH) and carbonyl (C=O) groups and adsorb on the particles' surface. The increase in the charge density shifts the isoelectric point (IEP) toward lower pH ranges and generates an electrostatic barrier that hinders their agglomeration.[25] In suspensions of heavier solid load (an arbitrary level is approximately 10 vol.%), the large ions dissociation enhances the ionic force of the medium and increases the interactions among particles. Therefore, even if the optimum dispersant content is used, relatively high apparent viscosity levels are attained, specially for the Al_2O_3-citrate system. (b) For FS20, on the other hand, the dispersion mechanism is electrosteric. Its molecular architecture is based on long and weakly charged main polymeric chains containing short and periodically spaced ramifications.[27,28] Therefore, its dispersion mechanism prevents particle agglomeration by combining physical impediment and electrostatic repulsion, does not affect their Zeta potential behavior significantly and is highly effective.

Similarly to equivalent systems described in other reports,[25–27,29] the Al_2O_3-FS20 suspension exhibited a pseudoplastic (reduction in the values of apparent viscosity as shear rate increases) and reversible (small differences on the levels of apparent viscosity in the two steps of the shear rate cycle) rheological behavior (Fig. 6b). The $Al(OH)_3$-FS20 one also behaved as a pseudoplastic fluid during the first part of the cycle as the shear rate is increased; however, when it was reduced, the apparent viscosity levels observed were significantly lower (particularly below 10 s^1). Assuming that the $Al(OH)_3$ particles were perfectly dispersed and individualized in the suspension before the beginning of the cycle, this effect can be attributed to their slight asymmetry.[30] As verified for other systems, suspensions containing plate-like particles (such as clay suspensions, for instance) may exhibit thixotropy. This time-dependent rheological behavior is generated by weak interactions amongst the particles that are formed when the suspension is static and that are easily broken at the first signs of movement. Under a constant shear rate condition, the physical consequence of this behavior is a sudden reduction in the apparent viscosity as a function of time; in shear rate cycles (such as the present case), it can be seen as significant differences in the viscosity levels, for a same shear rate, at distinct moments of the cycle. Further investigations that corroborate this hypothesis (such as oscillatory rheometry characterization), but that are also beyond the scope of this study, are under development in the authors' research group.

The cycles employed in the rheological characterization of the suspensions indicate that the $Al(OH)_3$-Al_2O_3 system can behave suitably under the shear rate levels typically found in the processing of castables structures.[30] Under the high shear rate (from 100 to 10 s^{-1}, Fig. 6b(i)) of the mixing step, both suspensions developed a pseudoplastic behavior and low levels of apparent viscosity, which are very useful to improve dispersion and particles deagglomeration. At medium shear rates (from 10 to 1 s^{-1}, Fig. 6b(ii)), the intermediate apparent viscosity levels enable the easy casting of the suspensions (vibration can be used to release trapped air bubble). Finally, at low shear rates (below 1 s^{-1}, Fig. 6(iii)) and after casting, the thixotropy observed for $Al(OH)_3$ avoids particles sedimentation and water segregation, as well as a faster strength gain when hydraulic binders are employed.

3.2. Microstructure and phase change (i) during thermal decomposition and (ii) at higher temperatures

For the grade of $Al(OH)_3$ tested under the described conditions, the thermal decomposition occurred between 208 °C and 370 °C (Fig. 4b), in an intense endothermic step (Fig. 4c), followed by a mass loss of 36.43%. Since the theoretical mass loss for $Al(OH)_3$ is 34.64%, the difference observed in the

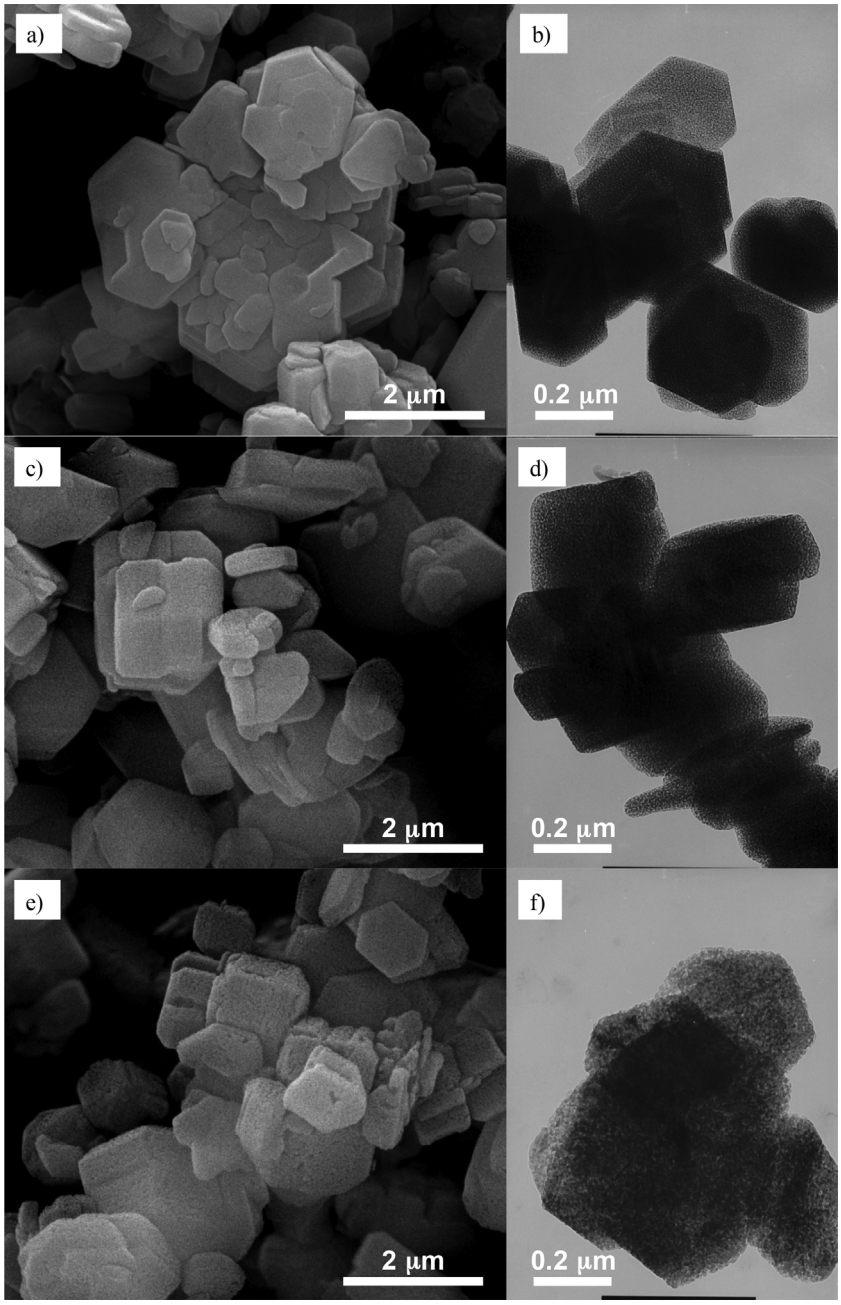

Fig. 8. SEM and TEM for $Al(OH)_3$ samples thermally treated at (a and b) 500 °C, (c and d) 700 °C and (e and f) 900 °C (5 °C min^{-1} heating rate, 5 h hold, 10 °C min^{-1} cooling rate).

experimental result can be attributed to the loss of physically adsorbed water. At 496 °C, there occurred a slight inflection at the base line, resulting from the beginning of the phase transformation of monoclinic gibbsite to hexagonal χ-Al_2O_3. The modifications continued up to higher temperatures, as seen in Fig. 2, however, because these are second order phase changes, no significant enthalpy variation was detected.

The largest increase in the specific surface area and pore volume verified was observed between the values achieved for the as-received material and the sample heated at 300 °C (Figs. 4a and 5a). During this intermediate stage of dehydroxilation, gibbsite was converted into boehmite (Fig. 2b) and experienced a huge crystallographic rearrangement and physical changes in its on particles' microstructure (formation of micro and meso pores, Fig. 1c and d). From 500 up to 700 °C, the topotactic formation of transition aluminas (χ-Al_2O_3, at 500–700 °C, and κ-Al_2O_3, 900 °C) of low crystallinity and large concentration of defects (Fig. 2c–e) is pointed out by progressively wider and less intense diffraction peaks.[12,13] During these phase changes, at the same time that density increases and SSA decreases (Fig. 4a), the total pore volume remains practically constant. This unusual behavior can be interpreted as a change in the shape and size of the microcracks formed during the dehydroxilation. At the early stages of sintering (900 °C), a fragmented porous surface is generated and each spot behaves as an individual and very reactive grain (average size around

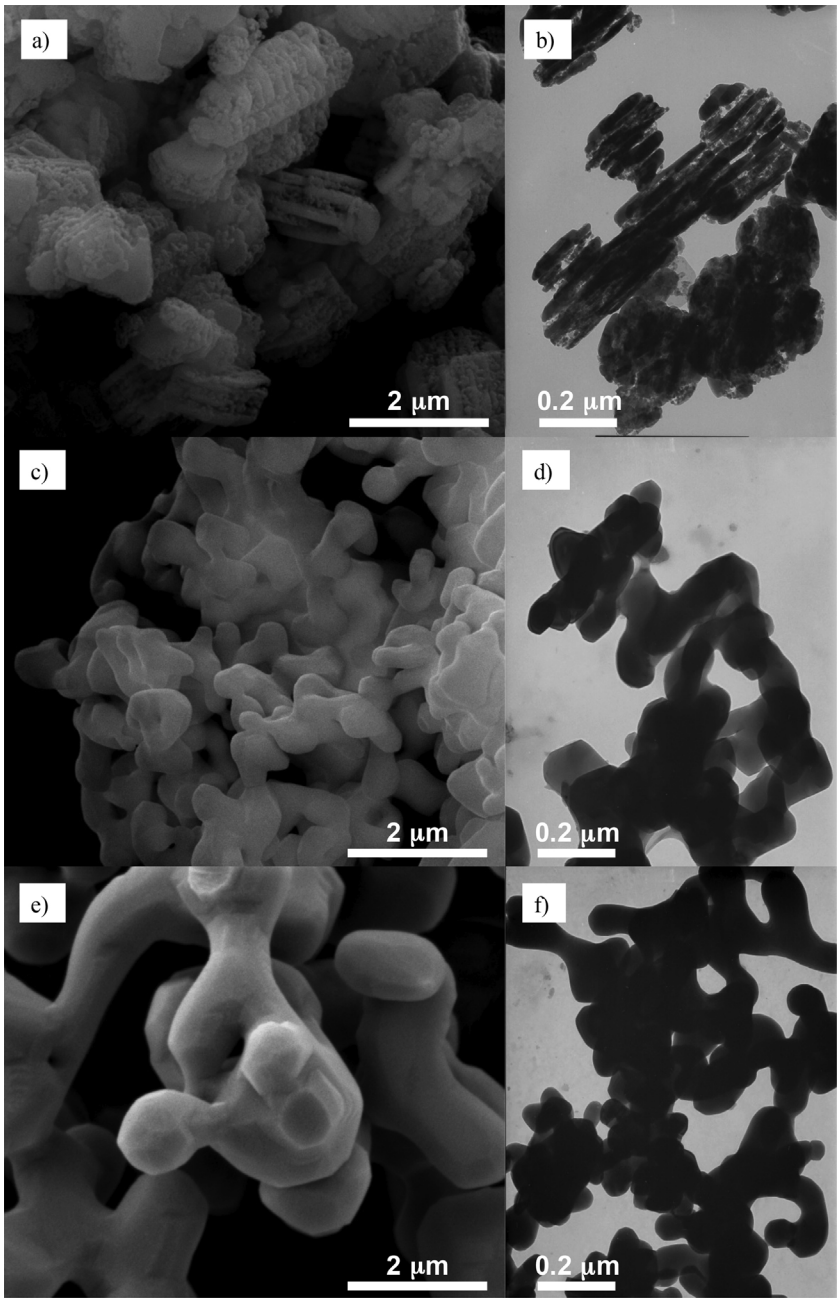

Fig. 9. SEM and TEM for $Al(OH)_3$ samples thermally treated at (a and b) 1100 °C, (c and d) 1300 °C and (e and f) 1500 °C (5 °C min^{-1} heating rate, 5 h hold, 10 °C min^{-1} cooling rate).

30–80 nm, Fig. 8e–f). Due to the high surface energy, these micrograins exert a huge driving force for the grain growth and sintering even at low temperatures as 700–900 °C.[7,10] Therefore, as heating continues: (i) the atomic rearrangement increases the solid density, (ii) cracks and grains merge, become thicker (Figs. 5b–c and 8e–f) and reduce SSA and, (iii) because of the low diffusion mobility, densification is not favored and the total pore volume remains practically constant.

At higher temperatures (1100–1500 °C), density stabilizes at around 3.5 g cm^{-3} and SSA and pore volume are drastically reduced (Fig. 4a) at the same time the first traces of the highly stable alpha-alumina (α-Al_2O_3, $2\theta = 43.3°$) appear (Fig. 2f). The full conversion to α-Al_2O_3 ends after a secondary recrystallization step at 1300 °C (Fig. 2g), above which no other phases are observed.[9] The merging and growing of cracks combined with the agglomeration and coarsening of the α-Al_2O_3 domains originate a co-continuous coral-like porous structure (Fig. 9). These α-Al_2O_3 filaments are almost completely dense (no significant content of inner micro or meso pores, Figs. 4a and 5d) and surrounded by elongated macroporous. Particularly for samples sintered at 1300 °C and 1500 °C, the boundaries of the original transition alumina grains still being seen (Fig. 9c–f). This is an indication that the system is an indication that the system has not yet reached its full stabilization despite the high temperatures of heat treatment.

4. Final remarks

The aluminum hydroxide ($Al(OH)_3$) grade tested showed suitable potential to be used as a porogenic agent in dense aluminum oxide (α-Al_2O_3) matrixes. $Al(OH)_3$ has dispersion and rheological compatibility with Al_2O_3, in a large extent of pH and even with the use of different dispersants. Such a compatibility is due to the similar size distribution and residual charge density on the surfaces of the particles, as pointed out by the Zeta potential measurements. These results indicate that castable Al_2O_3-$Al(OH)_3$ suspensions can be prepared with suitable solid load, after a proper dispersion and homogenization. During its thermal dehydroxilation (208–370 °C), $Al(OH)_3$ experienced a series of topotactic transformations, which generated a large surface area and inner porosity transition alumina phases, such as chi and kappa aluminas. The large quantity of pores (micro, meso and macro) originated (i) initially from the cracks produced during the water vapor withdrawal and (ii) from the volumetric shrinkage caused by the density increase (from 2.4 g cm^{-3} up to 3.7 g cm^{-3}). The pore content and specific surface area reached the highest levels after thermal treatments between 300 and 500 °C. Above this temperature interval, sintering events occurred and reduced the porosity and produced a coral-like co-continuous morphology. The following step in the development of castables porous thermal barriers based on the Al_2O_3-$Al(OH)_3$ system is its combination with a high refractoriness inorganic binder, such as hydratable alumina (ρ-Al_2O_3). This aspect is currently under investigation by the authors' research group.

Acknowledgements

The authors would like to acknowledge: (a) Brazilian Research Foundations FAPESP (2010/19274-5) and CNPq (470981/2011-3; 306036/2011-8) for supporting this study; (b) Almatis (Brazil and Germany) and BASF (Germany) for kindly supplying samples of raw materials and dispersant, respectively; (c) the Laboratory of Electron Microscopy of the Center for Hybrid Materials Technology (CTMH, IFSC and SMM/EESC), University of São Paulo (Brazil).

References

1. Santos PS. Natural aluminum oxides and hydroxides: a review. Part 2 – Gibbsite, bayerite, nordstrandite. *Cerâmica* 1985;**31**(182):29–36 (in Portuguese).
2. Wefers K, Misra C. *Oxides and hydroxides of aluminium –Alcoa technical paper, n. 19 (Revised)*. Pennsylvania: Aluminum Company of America; 1987. p. 54–8.
3. Jo YM. Characterization of ceramic composite membrane filters for hot-gas cleaning. *Power Technol* 1997;**91**(1):55–62.
4. Gallo JB, Agnelli JAM. Aspects of polymer behavior under fire conditions. *Polímeros: Ciência Tecnol* 1998;**8**(1):23–38 (in Portuguese).
5. Brown JF, Clark D, Elliott WW. The thermal decomposition of the alumina trihydrate gibbsite. *J Chem Soc* 1953:84–8.
6. Pandolfelli VC, Varela JA, Longo E. Physical, morphological and rheological modifications occurred during the calcination of aluminum hydroxide. *Cerâmica* 1987;**33**(206):89–98 (in Portuguese).
7. Zhou RS, Snyder RL. Structure and transformation mechanisms of the η, γ, and θ transition aluminas. *Acta Crystallogr* 1991;**B47**(1):617–30.
8. Levin I, Brandon D. Metastable polymorphs: crystal structures and transition sequences. *J Am Ceram Soc* 1998;**81**(8):1995–2012.
9. Santo PS, Santos HS, Toledo SP. Standard transition aluminas: electron microscopy studies. *Mater Res* 2000;**3**(4):104–14.
10. Deng ZY, Fukasawa T, Ando M, Zhang GJ, Ohji T. High-surface-area alumina ceramics fabricated by the decomposition of $Al(OH)_3$. *J Am Ceram Soc* 2001;**84**(3):485–91.
11. Mercury JMR, Pena P, Aza AH. On the decomposition of synthetic gibbsite studied by neutron thermodiffractometry. *J Am Ceram Soc* 2006;**89**(12):3728–33.
12. Coelho ACV, Santos HSS, Kiyohara PK, Marcos KNP, Santos PSS. Surface area, crystal morphology and characterization of transition alumina powders from a new gibbsite precursor. *Mater Res* 2007;**10**(2):183–9.
13. Gan BK, Madsen IC, Hockridge JG. In situ X-ray diffraction of the transformation of gibbsite to α-alumina through calcination: effect of particle size and heating rate. *J Appl Crystallogr* 2009;**42**(4):697–705.
14. Hongo Y. ρ-Alumina bonded castable refractories. *Taikabutsu Overseas* 1988;**9**(1):35–8.
15. Weiping M, Paul WB. Mechanisms of reaction of hydratable aluminas. *J Am Ceram Soc* 1999;**82**(2):453–6.
16. Kogure T. Dehydration sequence of gibbsite by electron-beam irradiation in a TEM. *J Am Ceram Soc* 1999;**82**(3):716–20.
17. Chevalier E, Chulia D, Pouget C, Viana M. Fabrication of porous substrates: a review of processes using pore forming agents in the biomaterial field. *J Pharm Sci* 2008;**97**(3):1135–54.
18. Salomão R, Brandi J. Macrostructures with hierarchical porosity produced from alumina-aluminum hydroxide-chitosan wet-spun fibers. *Ceram Int* 2013;**39**(7):8227–35.
19. Deng ZY, Fukasawa T, Ando M, Zhang GJ, Ohji T. Microstructure and mechanical properties of porous alumina ceramics fabricated by the decomposition of aluminum hydroxide. *J Am Ceram Soc* 2001;**84**(11):2638–44.
20. Li S, Li N. Effects of composition and temperature on porosity and pore size distribution of porous ceramics prepared from $Al(OH)_3$ and kaolinite gangue. *Ceram Int* 2007;**33**(4):551–6.
21. Salomão R, Vilas Bôas MOC, Pandolfelli VC. Porous alumina-spinel ceramics for high temperature applications. *Ceram Int* 2011;**37**(4):1393–9.
22. Salomão R, Souza ADV, Fernandes L, Sousa LL, Arantes VL. Porous ceramics in the Al_2O_3-$Al(OH)_3$ system. In: *Proceedings of the 13th Biennial Worldwide Congress on Refractories – UNITECR '13*. Victoria, Canada: The American Ceramic Society; 2013. p. 1028–33.
23. Santo PS, Coelho ACV, Santos HSS, Kiyohara PK. Hydrothermal synthesis of well-crystallised boehmite crystals of various shapes. *Mater Res* 2009;**12**(4):437–45.
24. Salomão R, Milena LM, Wakamatsu MH, Pandolfelli VC. Hydrotalcite synthsis via-coprecipitation reactions using MgO and $Al(OH)_3$ precursors. *Ceram Int* 2011;**37**(8):3063–70.
25. Studart AR, Pandolfelli VC, Tervoot E, Gauckler LJ. Gelling of alumina suspensions using alginic acid salt and hydroxyaluminum diacetate. *J Am Ceram Soc* 2002;**85**(11):2711–8.
26. Pileggi RG, Pardo ARF, Pandolfelli VC. Novel method for the selection of enhanced dispersants for refractory castables. *Cerâmica* 2002;**48**(308):206–11 (in Português).
27. Oliveira IR, Pandolfelli VC. Dispersants and their effects on hydratable alumina containing castables. *Refract Worldforum* 2009;**1**(1):103–9.
28. Salomão R, Souza ADM, Fernandez L, Arruda CC. Advances in nanotechnology for refractories: when very small meets hot, heavy, and large. *Am Ceram Soc Bull* 2013;**92**(7):22–7.
29. Ortega FS, Castro RHR, Gouvêa D, Pandolfelli VC. The rheological behavior and surface charging of gelcasting alumina suspensions. *Ceram Int* 2008;**34**(1):237–41.
30. Schramm G. *A practical approach to rheology and rheometry*. 2nd ed. Karlsruhe: Gebrueder HAAKE GmbH; 2000.